Journal of Engineering, Science and Technological Trends (JESTT)
Vol. 1, Issue 2, August 2024
DOI: https://doi.org/10.48112/jestt.v1i2c.1

Article

An Insight into Optical Constants of Iron Phenanthroline Molecules

Hayder Fahim[1&2*], Hashim Jabbar[1] and Adil A. Al-Fregi[1]

[1]University of Basrah, College of Science, Iraq

[2]Kerbala University, College of Education for Pure Science, Iraq

* Corresponding Email: hyder.fahem@uokerbala.edu.iq (H. Fahim)

Received: 07 November 2023 / Revised: 11 July 2024 / Accepted: 17 July 2024 / Published Online: 31 August 2024

ABSTRACT

In this study, we investigate the optical properties of Iron 1,10-phenanthroline molecular nanolayer synthesized were prepared using the complexation reactions method. Fe^{2+}(Phen) molecular thin films were then prepared as samples and subsequently characterized using XRD and UV-Vis spectroscopy. The main objective of this work is to explore the optical constants relevant to the light-induced spin crossover phenomenon in this molecule. UV-Vis study of nanometer thickness layer (100 nm) at wavelength $(200 - 1100\ nm)$, the distribution of refractive index is discussed in the framework of the single oscillator Wemple-DiDomenico model and various distribution parameters such as single oscillator energy (E_o), dispersion energy (E_d), refractive index ($n_{(0)}$), and optical absorption based on absorption edges dielectric constant (ε_∞) using Miller's rule. The moment of the dielectric constant optical spectrum (M_{-1}, M_{-3}) and energy gap by Wemple-DiDomenico approximation (E_g^{WDD}) have been computed, as has non-linear optical susceptibility ($\chi^{(3)}$), direct energy gap by Tauc relation (E_g^T), and Urbach energy of the localized states (E_u).

Keywords*:* Fe^{2+}(Phen) Molecular; Iron 1; 10-phenanthroline; Ligand Exchange Synthesis Method; Spin Crossover Phenomenon

1. Introduction

The photophysical characteristics of $Fe(II)$ complexes containing polyimine ligands, such as $[(Fe(phen)_3]^{2+}$ $(phen = 1{,}10 - phenanthroline)$, have recently gained considerable attention [1]. These investigations are fundamentally important for understanding photophysics in $3D$ transition metal complexes, but they also have applications in comprehending optical writing/magnetic reading in spin crossover (SCO) compounds [2]. Furthermore, such compounds were considered as possible replacements for $Grätzel - type$ dye-sensitized photovoltaic cells [3]. Indeed, these diamagnetic low-spin d^6diimine complexes are thought to be models for $Fe(II)$ SCO complexes with N_6 coordination spheres based on heteroaromatic ligands. In comparison, SCO complexes typically have a substantially lower zero-point energy differential H_{HL} $(1000\ cm^{-1})$ between the $high - spin\ (HS)$ and $low - spin\ (LS)$ configurations with low ligand-field (LF) strength [4],[5]. The Light-Induced Excited Spin State Trapping $(LIESST)$ phenomenon is known for SCO complexes in which the low temperature LS ground state can be photoconverted to a long-lived metastable HS state in the solid state [6],[7]. It was previously demonstrated that such photoconversion might occur in solution at roughly room temperature utilizing pulsed irradiation and associated rapid relaxations [8]. Despite possessing a significantly higher H_{HL} $(6000\ cm^{-1})$, $Fe(II)$ LS polyimine complexes display the same conversion to a metastable HS state by ultrafast optical pumping, with even quicker matching relaxations [1],[4],[6] While these compounds have many intriguing optical properties, their usage in optics is currently limited due to the centrosymmetry that most $Fe(II)$ complexes with polyimine ligands have in solid state. This centrosymmetry precludes these compounds from showing fascinating features such as piezoelectric and electro-optic effects, as well as second order non-linear optical phenomena resulting in second harmonic and sum frequency creation. To broaden the use of $Fe(II)$ complexes, their inherent centrosymmetry must be broken [9],[10].

2. Experimental Part

Iron (II) complexes derived 1,10-phenanthroline (d^6) are arguably the most well-studied examples of spin-crossover

compounds due to the large change in magnetism that results from transitions between the low-spin, diamagnetic (S = 0) state to a high-spin (S = 2) state. So, in the present study, we will prepare three low spin- F(II) complexes containing both nitrogen and sulfur donor atoms with the general formula $[Fe(phen)_x(SCN)_y]_{c+}$ {x= 0, 1, 2, 3; y=0, 2, 4} and examined the spin crossover of these complexes.

A solution of ascorbic acid (approximately 10 g diluted in 20 mL of distilled water) was added drop by drop to the ferrous sulfate solution to create fresh $FeSO_4.7H_2O$. After the colour of the solution was changed to a light blue, the solution was allowed to cool to room temperature. After that, 20 mL of ethanol was added to afford ferrous sulfate hydrate $FeSO_4.7H_2O$ as light blue in 95% yield.

2.1. Preparation of bis (phenanthroline) dithiocyanatoiron (II) $Fe(Phen)_2(SCN)_2$

A solution (0.468 g, 2 mmol) of 1,10-phenanthroline hydrochloride monohydrate, in 20 mL of distilled water was added drop by drop to an aqueous solution of (0.278 g, 1 mmol), ferrous sulfate heptahydrate, in 15 mL of distilled water with gentle stirring. The mixture was stirred at room temperature for 3 hours. Then, a solution of 0.152 g, 2 mmol) of ammonium thiocyanate, NH_4SCN, was added. The reaction mixture was stirred for 3 hours to obtain a dark red colour which was then collected by filtration. The crude solid was washed several times with distilled water and ethanol to obtain red crystals of bis (phenanthroline) dithiocyanatoiron(II) $[Fe(Phen)_2(SCN)_2]$ in an 89% yield.

2.2. Preparation of Tris(phenanthroline) iron(II) sulfate $[Fe(Phen)_3]SO_4$

A mixture of light blue crystals of (0.278 g, 1 mmol) ferrous sulfate heptahydrate, $FeSO_4$ .7H2O and (0.702 g, 3 mmol) 1,10-phenanthroline hydrochloride monohydrate, in 25 mL of distilled water was stirred at room temperature for 3 hours. A red solution was formed which was then, reduced by a rotary evaporator to obtain a red solid. The crude solid was washed several times with ethanol to obtain red crystals of tris(phenanthroline)iron(II) sulfate in 93% yield.

2.3. Preparation of ammonium phenanthrolinetetra thiocyanatoferrate(II) $(NH_4)_2[Fe(Phen)(SCN)_4]$

A solution of 1,10-phenanthrolinium hydrochloride monohydrate, (0.234 g, 1 mmol) in 20 mL of distilled water was added slowly and drop by drop to the aqueous solution of ferrous sulfate heptahydrate, (0.278 g, 1 mmol), in 15 mL of distilled water. The mixture was stirred at room temperature for 1 hour. Then, a solution of ammonium thiocyanate, NH_4SCN, (0.304 g, 4 mmol) was added. The reaction mixture was stirred for 3 hours to obtain a dark red color solution which was then dried by rotary evaporator to dryness. The crude solid was washed several times with ethanol red crystals of ammonium phenanthroline tetra thiocyanato ferrate (II) $(NH_4)_2[Fe(Phen)(SCN)_4]$ in 77% yield.

2.4. Preparation of Ammonium hexathiocyanatoferrate(II) $(NH_4)_4[Fe(SCN)_6]$

A solution of (0.456 g, 6 mmol) ammonium thiocyanate in 20 mL of distilled water was added to an aqueous solution of (0.278 g, 1 mmol), ferrous sulfate heptahydrate, in 25 mL of distilled water with gentle stirring at room temperature for 3 hours. A darkened colour solution was obtained and then dried by a rotary evaporator to dryness. The crude solid was washed several times with ethanol to obtain red crystals of ammonium hexahiocyanatoferrate (II) $(NH_4)_4[Fe(SCN)_6]$ of about 92% yield.

2.5. Layer thin films of phenanthroline molecular using spin-coating

1- Fe $(phen)_2$ $(SCN)_2$ have been dissolved in ethanol to make a concentration of 0.1-1.0 mM.
2- The substrate was cleaned using ultrasonication for 10 min, Acetone, Ethanol, and N_2 gun.
3- solution was dropped onto the substrate, during rotation at 2000-4000 rpm for 30-60 s.
4- The samples were dried under a vacuum for 1–2 h to evaporate the solvent and to form a uniform thin film.

Optimization of preparation conditions such as solvent selection, concentration, spin speed, and duration can affect the properties of the thin film. The glass was employed as a substrate to create a thin film of the mentioned materials with a thickness of 100 nm, thickness was measured with a profilometer [F20-FilMetrics], and absorbance, transmittance, and reflectivity were measured by UV-Vis spectrophotometer. [Shimazdu - (UV-1800) - (1100-190) nm- Physics department/ Basrah University].The structural and optical characteristics of iron (phen) thin films were examined with $X-ray$ diffraction(XRD).

3. Results and discussion

The phase formation investigation was performed using an $XPERT-PRO\ X-ray$ diffractometer (XRD) with $Cu-K\alpha$ radiation ($\lambda = 1.54$ Å) over the range $2\theta \sim 10-80°$ with a step size of 0.02° . The results of $X-ray$ diffraction of $iron\ (phen)$ thin films were shown the crystal structure revealed by XRD of the SCO films at room temperature, it should be mentioned that the JCPD card for $Fe(phen)_2(SCN)_2$, $(NH_4)_2[Fe(phen)(SCN)_4]$, $(NH_4)_4[Fe(SCN)_6]$, and $[Fe(phen)_3]SO_4$ molecules is not available in the literature.

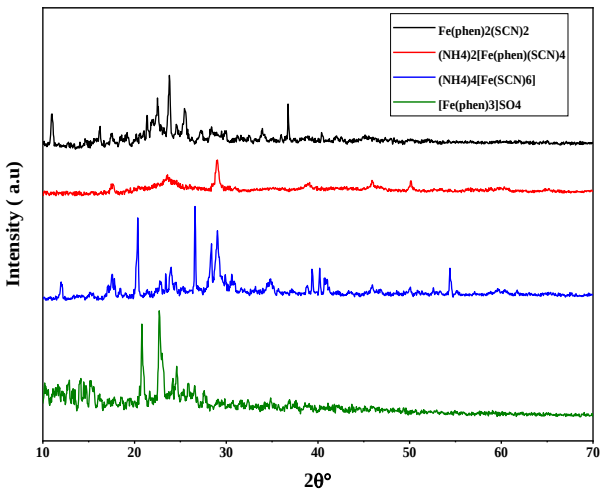

Figure 1: *The X-ray diffraction (XRD) pattern illustrating the diffraction behaviour of nanocrystals within the Fe (phen) thin films. This diffraction occurred on glass substrates at room temperature and a thickness of 100 nm.*

The XRD pattern in (Figure 1) provides information about the crystal structure of the thin films. By comparing the obtained diffraction peaks with the selection of Bragg peaks from Table 1

for different complexes, we can deduce the crystallographic phase present in the Fe(phen) thin films. Here's an explanation of the results based on the provided Table 1:

1. $Fe(phen)_2(SCN)_2$: The average crystal size is approximately 33.16 Å. The diffraction peak positions at various 2θ angles correspond to specific crystallographic planes within the $Fe(phen)_2(SCN)_2$ complex. The multiple peaks observed suggest that the thin film contains a crystalline phase with well-defined crystallographic orientations.

2. $(NH_4)_2[Fe(phen)(SCN)_4]$: The average crystal size is about 18.62 Å. The observed diffraction peaks correspond to specific crystallographic planes within the (NH4)2[Fe(phen)(SCN)4] complex. These peaks indicate the presence of a distinct crystalline structure in the thin film.

3. $(NH_4)_4[Fe(SCN)_6]$: The average crystal size is approximately 32.43 Å. The observed diffraction peaks align with specific crystallographic planes of the (NH4)4[Fe(SCN)6] complex. These peaks indicate the presence of a certain crystalline arrangement within the thin film.

4. $[Fe(phen)_3]SO_4$: The average crystal size is around 37.93 Å. The diffraction peaks observed at specific 2θ angles correspond to crystallographic planes within the [Fe(phen)3]SO4 complex. These peaks suggest the presence of a distinct crystalline phase within the thin film.

In summary, the XRD pattern reveals the presence of well-defined crystallographic phases in the Fe(phen) thin films, which correspond to the different complexes mentioned. The diffraction peaks and their positions provide insights into the arrangement of atoms within the crystal lattice of the thin films[11].

Table 1:
Selection of Bragg peaks extracted from X-ray diffractograms

Complexes	Average crystallite size (XRD) (nm)	The diffraction peak position (2θ°)
$Fe(phen)_2(SCN)_2$	33.16	11.02, 13.41, 14.70, 16.22, 17.55, 19.22, 21.40, 22.10, 22.55, 23.82, 24.62, 25.53, 27.27, 28.44, 29.08, 29.90, 32.53, 33.99, 36.02, 36.80, 38.83, 40.48, 42.17, 45.45
$(NH_4)_2[Fe(phen)(SCN)_4]$	18.62	17.60, 23.60, 29.03, 38.97, 45.96, 50.15, 59.97, 65.00
$(NH_4)_4[Fe(SCN)_6]$	32.43	12.06, 13.97, 15.30, 17.63, 18.47, 20.36, 21.41, 22.86, 23.44, 24.00, 25.31, 26.63, 28.37, 29.05, 30.72, 34.79, 38.84, 39.43, 40.23, 40.90, 46.00, 50.05, 54.46, 59.88
$[Fe(phen)_3]SO_4$	37.93	10.35, 11.56, 12.85, 14.08, 14.50, 15.25, 20.84, 22.75, 24.63, 25.89, 26.57, 27.62, 36.90, 38.88

Through the application of the Scherrer equation, the association is expressed as follows: (τ = (K * λ) / (β * Cos(θ)), wherein: τ stands for the nanoparticle's size. K represents a dimensionless constant, contingent on the crystal's shape, often falling within the range of about 0.9. β signifies the apex width at the mean height. θ corresponds to the Bragg angle. Lastly, λ denotes the wavelength, measured in nanometers [12].

The ligand and the iron complex both play crucial roles in terms of absorbance due to their interaction with light. The ligand contains specific functional groups that can absorb light at certain wavelengths, leading to distinct absorption bands in the spectrum. On the other hand, the iron complex can also contribute to absorbance as the central iron ion and its surrounding structure can influence the energy levels of electrons, causing them to absorb light at particular wavelengths. In essence, both the ligand and the iron complex contribute to the overall absorbance spectrum through their unique electronic properties and interactions with photons.The interaction between electromagnetic radiation and a thin film's material during absorption results in changes in the absorption spectra. These spectra provide information about the electronic configurations of the material and can be analyzed using UV-Vis absorption for studying electron-radiation interactions. Alternatively, infrared absorption is frequently employed to investigate the interaction between bond vibration energy and electromagnetic waves.

Within this context, the absorption (A) and the transmittance (T) spectra for $Fe(phen)$ thin films were recorded in the wavelength range of $(200 - 1100nm)$. The reflection (R) can be determined using the following relation[13]:

$$T = \frac{(1-R)^2 e^{-\alpha d}}{1-R^2 e^{-2\alpha d}} \qquad (1)$$

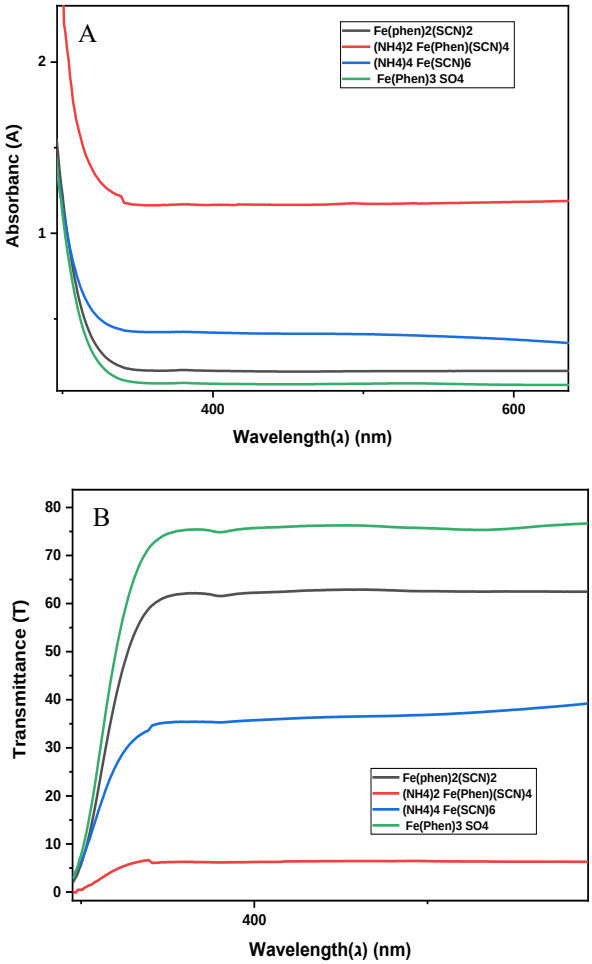

Figure 2: *The relationship between A- absorbance wavelength, B-transmittance and wavelength for Fe (phen) thin films at thickness 100 nm.*

Where T is transmittance, $\propto$ is the absorption coefficient, and d is the thickness of the sample. From the absorption coefficient data, extinction coefficient (K) can be calculated by:

$$K = \frac{\alpha\lambda}{4\pi} \qquad (2)$$

The refractive index (n) can be calculated using the following relation:

$$R = \frac{(n-1)^2+K^2}{(n+1)^2+K^2} \qquad (3)$$

Absorbance is a measure of how much light a material absorbs at a specific wavelength. In the context of the Fe (phen) thin films, the absorbance plot (A) illustrates how the films interact with light of different wavelengths. The molecular structure of the films and the electronic energy levels of their components play a crucial role in these interactions. When light passes through the thin films, it can be absorbed by the molecules present in the films. This absorption occurs due to electronic transitions, where electrons within the molecules are excited from lower energy levels to higher energy levels by absorbing photons of specific energies corresponding to certain wavelengths. The energy difference between these levels matches the energy of the incoming photons.

In the absorbance plot, peaks and valleys indicate the wavelengths at which these electronic transitions are most likely to occur. A peak represents a wavelength where the thin films absorb light most strongly because it corresponds to an energy level difference that matches the energy of the photons. These peaks are characteristic of the electronic structure of the molecules within the films.

Transmittance measures the fraction of light that passes through a material without being absorbed. In the transmittance plot (B), higher values indicate that the thin films are allowing more light to pass through, while lower values suggest that the films are absorbing more light. The relationship between absorbance and transmittance is complementary. If a material absorbs a significant amount of light at a certain wavelength (high absorbance), it will have low transmittance at that wavelength. Conversely, if a material absorbs very little light at a certain wavelength (low absorbance), it will have high transmittance at that wavelength. In the context of the Fe (phen) thin films, regions of high absorbance correspond to regions of low transmittance, and vice versa. The peaks in the absorbance plot align with the valleys in the transmittance plot. This indicates that the thin films are absorbing light strongly at those wavelengths, leading to reduced transmission of light through the films.

In summary, the absorbance and transmittance plots in Figure 2 provide a detailed picture of how the Fe (phen) thin films interact with light. The peaks in absorbance signify electronic transitions within the molecules, while the valleys in transmittance indicate regions where the films are absorbing light. Together, these plots offer insights into the molecular and electronic properties of the thin films.

The refractive index of a material, which can be determined using UV-visible absorption spectra, characterizes the path of light through the material as shown in Figure 3. A higher refractive index leads to greater deviation of light within the material. This optical constant is of great importance in the design of optical devices and provides key information about the material's optical properties, including its local field, polarization, and phase velocity of light. Refractive index:

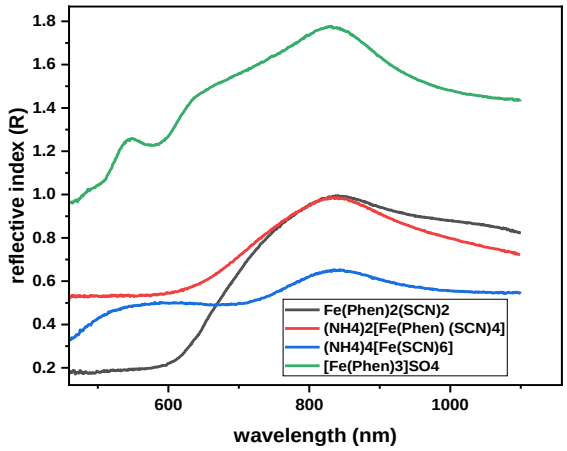

Figure 3: *The relationship between reflective index (R) and wavelength for Fe (phen)thin films at thickness 100 nm.*

$$\boldsymbol{n = \frac{1}{T_s} + \sqrt{\frac{1}{T_s - 1}}} \qquad (4)$$

Where $T_s = 10^{-A} * 100$, n : Refractive index, T_s=Transmittance, A: Absorbance. Now we have to plot a graph that shows variation in refractive index as a function of wavelength of light.

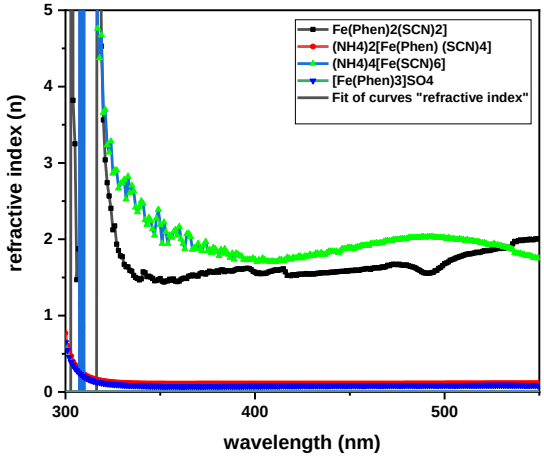

Figure 4: *The relationship between refractive index (n) and wavelength (λ) for thickness 100 nm, The symbols represent the experimental outcomes, while the solid lines depict the model fit data using the Sell Meier dispersion function.*

This graph shows that the refractive index initially decreases and then increases to its maximum value. After approaching this peak value, again it decreases. The observed distortion is attributed to the influence of the glass on the absorption edge around the wavelength of 300 nm and its adjacent region.

Figure 4 illustrate the refractive index values for different wavelengths (λ), which are commonly used to describe the optical properties of solids. The complex dielectric function $\varepsilon(E) = \varepsilon_1(E) + i\varepsilon_2(E)$, is a crucial tool for understanding these properties, as it provides frequency-dependent information about both the real part ε_1 and imaginary part ε_2. The quantity ε_2 is particularly significant, as it captures physical information about the material, including interband transitions at high energies $E \gg E_g$, interband transitions near the absorption edge, free carrier

absorption, and optical phonon absorption. The real part of the dielectric constant is the sum of these contributions, with K being negligible in the transparent region, leading to normal dispersion [14]. According to the single oscillator model, the dielectric constant (ε_1) dispersion is caused solely by interband transition and assumes that each electron acts as an oscillator [15]. Therefore, the dielectric constant (ε_1) can be expressed as:

$$\varepsilon_1(\omega) = 1 + \frac{F}{E_o^2 - (\hbar\omega)^2} \qquad (5)$$

The dielectric constant of a material can be calculated using the Wemple-DiDomenico model (WDD), which defines the parameter F as $F=E_dE_o$, where $E_d$represents dispersion energy and $E_o$represents single-oscillator energy. This model is based on the single-oscillator approximation, where E_o and F are parameters determined by the electric dipole oscillator. Thus, the dielectric constant can be expressed as a function of these parameters, as given in equation [16],[17].

$$\varepsilon_1(\omega) = n^2(\omega) - 1 = \frac{E_oE_d}{E_o - (\hbar\omega)^2} = \frac{E_d}{E_o}\left[1 - \frac{(\hbar\omega)^2}{E_o^2}\right]^{-1} \qquad (6)$$

The strength of interband optical transition and the chemical bonding in the unit cell are closely related to the dispersion energy E_d. On the other hand, the dispersion parameter E_d is commonly considered an "average" energy gap (E_g^{WDD}) and is empirically correlated with the lowest direct Tuac energy gap (E_g^T). The dispersion parameters E_o and E_d are determined using the r^{th}moment of the optical spectrum $\boldsymbol{\varepsilon_2(E)}$. The r^{th} moment of the $\boldsymbol{\varepsilon_2(E)}$spectrum can be defined as per [15][17]:

$$M_r = \frac{2}{\pi}\int_{E_t}^{\infty} E^r \varepsilon_2(E)dE \qquad (7)$$

Here, $E = \hbar\omega$ and E_t represents the energy threshold for absorption. Relationships between the dispersion parameters and $\boldsymbol{\varepsilon_2}$ (ω) spectrum can be established through:

$$E_o^2 = \frac{M_{-1}}{M_{-3}} \qquad (8)$$

$$E_d^2 = \frac{M_{-1}^3}{M_{-3}} \qquad (9)$$

Where $M_{-1}$and M_{-3} represent the moments of the optical spectrum, and the -1 and -3 moments are used to calculate E_o and E_d [16]. The static dielectric constant of any material is defined as:

$$\varepsilon_r(o) = \mathrm{Lim}_{E\to o} n^2(E) = n_o^2$$

The static dielectric constant can be expressed in terms of the dispersion parameters as follows:

$$n_o^2 = \varepsilon_r(o) = 1 + \frac{E_d}{E_o} \qquad (10)$$

The values of E_o andE_d can be obtained by plotting $(n^2 - 1)^{-1}$ against $(h\nu)^2$ and finding the gradient $(E_dE_o)^{-1}$ and the intercept (E_o/E_d) on the vertical axis, as illustrated in Figure 8. Table 1 provides the values of E_o, E_d, M_{-1}, M_{-3}, $n(o)$, and $\boldsymbol{\varepsilon}(\infty)$.$E_o$represents the distance between the centres of the valance and conduction bands. The Wemple-DiDomenico model can also be used to calculate the value of E_g^{WDD}, which is listed in Table 2. In the visible, nonlinear, and near-infrared regions, the Muller rule is a useful tool for equalizing the third-order nonlinear polarizability parameter ($\chi^{(3)}$) according to Wagner et al.[18], using the equation [16] :

$$\chi^{(3)} = A\left(\chi^{(1)}\right)^4 = A[E_oE_d/4\pi(E_o^2 - (h\nu)^2]^4 = \frac{A}{(4\pi)^4(n^2-1)^4} \qquad (11)$$

Where: $A = 1.7x10^{-10}$. **Figure 5** illustrates the third-order nonlinear optical susceptibilities for thicknesses of Fe (phen) thin films, which were calculated using equation (11).

Studying the optical absorption spectrum is a simple and effective method to explore the band structure of semiconducting materials. It involves analyzing the changes in transmitted light intensity with wavelength, which can reveal quantum mechanical transitions that electrons in the semiconductor may undergo. By doing so, researchers can gain insights into the distribution of allowed electronic energy levels. The Tauc relation [19] is commonly used to analyze the strong absorption region, where α increases linearly with increasing photon energy, and it provides a relationship between the absorption coefficient and photon energy. This relationship allows researchers to extract crucial information such as the band gap energy and Tauc exponent, which can provide details about the type of semiconductor, degree of disorder, or presence of impurities/defects [20].

$$\alpha h\nu = B\left(h\nu - E_g^T\right)^r \qquad (12)$$

According to the given equation, B is a constant and E_g^T is the Tauc energy gap, with the variable *r* being an index characterizing the absorption process. In a study of thin solid films of Fe(phen), it was found that *r = 2* for the direct band gap and *r = 1/2* for the indirect band gap. Plotting $(\alpha h\nu)^2$ against *hν* showed that the best fit was a linear relation given by equation (12), suggesting that the interband transition in Fe(phen) thin films is due to the indirect transition. The optical Tauc band gap for Fe(phen) thin films was obtained by plotting $(\alpha h\nu)^2$ against hν in Figure (6) and extrapolating the linear region of the plot where ($\alpha h\nu = 0$). The absorption coefficient is a measure of the material's ability to absorb light per unit length and is affected by various factors such as composition, structure, purity, and the wavelength of the incident light. Analyzing the absorption coefficient as a function of wavelength can provide information about the material's electronic and optical properties, including energy levels and band structure.

Absorption Coefficient: $\alpha = \frac{2.303*A}{l}$ (13)

Where: α: Absorption Coefficient, A: Absorbance, l: Thickness of thin film

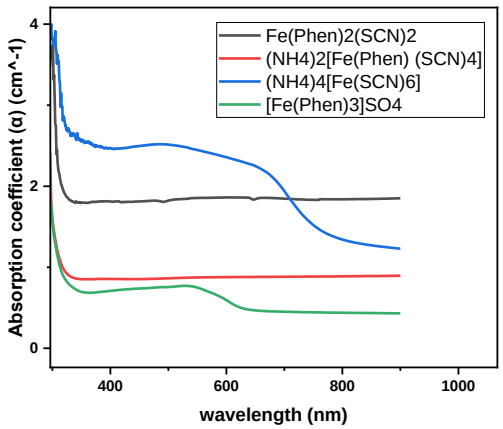

Figure 5: *The relationship between absorption coefficient (α) and wavelength for Fe(phen) thin films at thickness 100 nm.*

The absorption coefficient graph exhibits an atypical pattern, where absorption initially rises and then declines. This anomaly could be due to several factors, including the presence of impurities or defects within the material, surface roughness or scattering effects, or interference effects that arise from the interaction of light with the material's structure. To pinpoint the exact mechanisms accountable for this behaviour, additional analysis and characterization are necessary. In non-crystalline materials, defects could also be a factor.

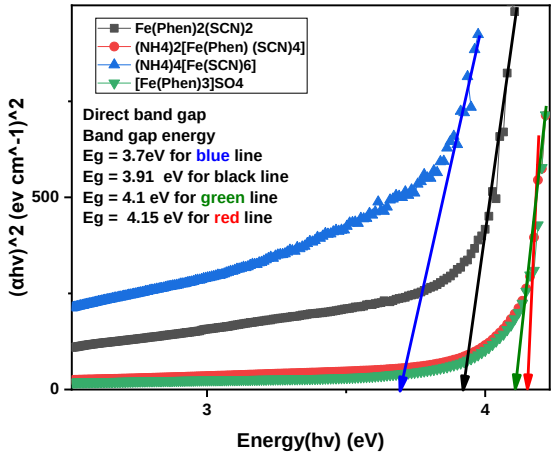

Figure 6: *The relationship between(αhv)²and photon energy for directFe (phen) thin films at thicknesses 100 nm*

The information provided suggests that the direct band gap graph is the most suitable method for extrapolating data on the x-axis shown in Figure 6. Analysis of the graph reveals that $Fe(phen)_2(SCN)_2$ has an energy gap value of 3.91eV, while $(NH_4)_4[Fe(SCN)_6]$, $(NH_4)_2[Fe(phen)(SCN)_4]$, and $[Fe(phen)_3]SO_4$ have energy gap values of 3.7 eV, 4.15eV and 4.1 eV, respectively. This indicates that $Fe(phen)_2(SCN)_2$, which contains Iron 1,10-phenanthroline molecular, has a smaller energy gap. However, it is important to acknowledge that other factors can impact the energy gap value. Therefore, when studying direct Fe(phen) thin films at a thickness of 100 nm, it is necessary to consider additional factors beyond the relationship between photon energy and constants depicted in the direct band gap graph. In summary, the topic revolves around examining the relationship between photon energy and constants for direct Fe(phen) thin films at a thickness of 100nm. The direct band gap graph is used for extrapolation on the x-axis, and the results highlight a smaller energy gap for $Fe(phen)_2(SCN)_2$, although other factors can also influence the energy gap value. The dielectric constant is a significant characteristic of optical materials, which are made up of both Real and Imaginary parts. It offers information about the permittivity and polarizability of a substance, which is related to the density of states within the forbidden energy gap.

The Real part of the dielectric constant indicates the extent to which the speed of light can be slowed down in the material, while the Imaginary part indicates the absorption of energy by an electric field due to dipole motion. To calculate both the real and imaginary parts of the dielectric constant from UV-visible absorption data:

$$\varepsilon_r = n^2 - k^2 \qquad (14)$$
$$\varepsilon_i = 2nk \qquad (15)$$

The formula for Urbach Energy (Eu), which is $\propto = \propto_\circ \mathbf{exp}\left(\frac{hv-Eg}{Eu}\right)$, can be rewritten as:

$$\boldsymbol{ln}\propto = \frac{1}{Eu}\boldsymbol{hv} - \frac{Eg}{Eu} + \boldsymbol{ln}\propto_\circ \qquad (16)$$

This equation is similar to the straight-line equation:

$$y = mx + c \qquad (17)$$

By comparing these two equations, we can see that the slope of the line in equation 16 is equal to one over the Urbach energy, the y-axis represents $\boldsymbol{ln}\propto$, and the x-axis represents $\boldsymbol{hv}$. The constant term in equation 16 corresponds to the y-intercept. Therefore, if we graph $\boldsymbol{ln}\propto$ on the y-axis and $\boldsymbol{hv}$ on the x-axis, the slope of the line will give us the inverse of the Urbach energy.

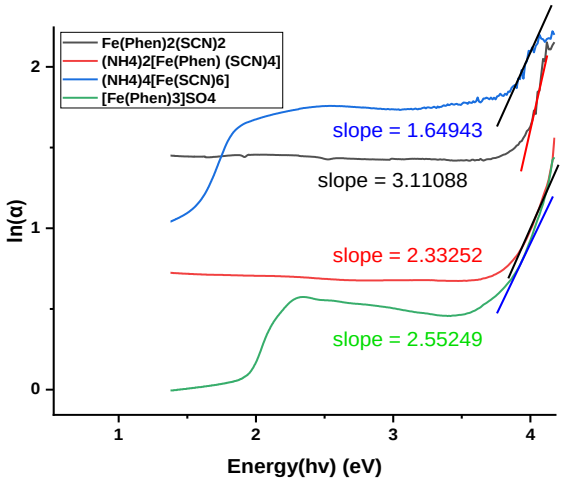

Figure 7: *The relationship between the ln(∝) and photon energy*

Now the slope of $(Fe(phen)_2(SCN)_2)$ comes out to be (3.11088). Put this value to get the $Urbach\ energy$ in eV. Thus, Urbach energy comes out to be (0.321 eV) or (321 meV) shown in Figure 7. And the slope of$((NH_4)_4[Fe(SCN)_6])$comes out to be (1.64943). Put this value to get the Urbach energy in eV. Thus, $Urbach\ energy$ comes out to be (0.606eV) or (606 meV). And the slope of $((NH_4)_2[Fe(phen)(SCN)_4])$ comes out to be (2.33252). Put this value to get the Urbach energy in eV. Thus, $Urbach\ energy$ comes out to be (0.428 eV) or (428 meV). And the slope of $([Fe(phen)_3]SO_4)$ comes out to be (2.55249). Put this value to get the Urbach energy in eV. Thus, $Urbach\ energy$ comes out to be (0.391eV) or (391 meV).

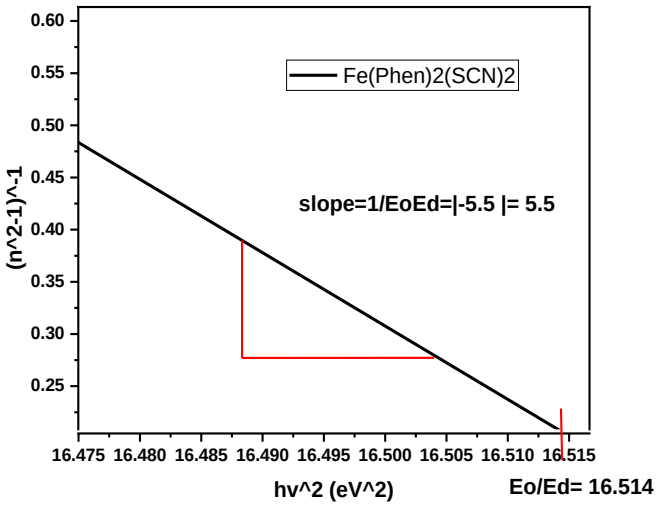

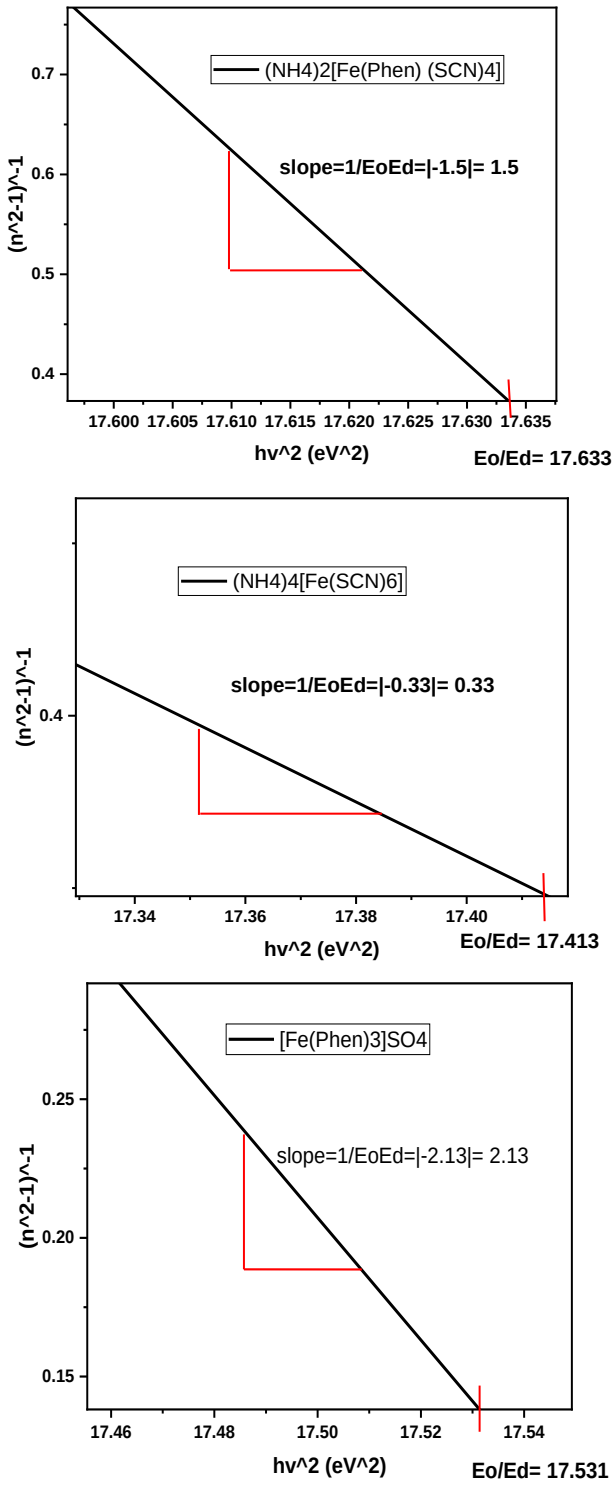

Figure 8: *The relationship between* $(hv)^2$ *and* $(n^2-1)^{-1}$

The Urbach energy is a parameter used to describe the width of the tail of the exponential absorption edge of a semiconductor material. It characterizes the degree of disorder and structural imperfections in the material, such as defects and impurities. When the Urbach energy decreases, it means that the tail of the absorption edge becomes narrower, indicating that the material has fewer structural imperfections and is more ordered. This can result in higher carrier mobility and improved optical properties, such as increased transparency and reduced absorption losses [19]. Band gap energy is the difference in energy between the valence band and the conduction band of a solid material.

Table 2:
The estimated values of the oscillator parameters of Fe (phen)thin films

Complexes	Oscillation Energy E_o(eV)	Dispersion Energy E_d(eV)	Field strength (f) $(eV)^2$	$n^2(o)$	ε_∞	M_1 (eV)	M_3 (eV)
$Fe(phen)_2(SCN)_2$	1.7338	0.1049	0.1818	1.06	1.029	0.06	0.02
$(NH_4)_2[Fe(phen)(SCN)_4]$	3.4163	0.1944	0.6641	1.057	1.028	0.056	0.005
$(NH_4)_4[Fe(SCN)_6]$	7.2541	0.4175	3.0285	1.057	1.028	0.057	0.001
$[Fe(phen)_3]SO_4$	2.8715	0.1637	0.47	1.057	1.028	0.039	0.0047

$E_g^{WWD} \approx E_o$

Table 3:
The calculated values of energy gap by Wemple-DiDomenico approximation, Tauc relation and calculated values of Urbach tails energy

Complexes	$E_g^{WWD}(eV)$	$E_g^T(eV)$	$E_u\,(meV)$
$Fe(phen)_2(SCN)_2$	1.7338	3.91	321
$(NH_4)_2[Fe(phen)(SCN)_4]$	3.4163	4.15	428
(NH4)4[Fe(SCN)6]	7.2541	3.7	606
$[Fe(phen)_3]SO_4$	2.8715	4.1	391

According to Figure 9, the peak values of susceptibilities ($\chi^{(3)}$) are$1.67 * 10^{-15}$ surf $(Fe(phen)_2(SCN)_2)$,$7.17 * 10^{-15}$ surf $(NH_4)_2[Fe(phen)(SCN)_4]$,$3.25 * 10^{-7}$ esu of $(NH_4)_4[Fe(SCN)_6]$ and $7.05 * 10^{-15}$ esuof $[Fe(phen)_3]SO_4$). The figure illustrates the relationship between the third-order nonlinear optical susceptibility and photon energy. Experimental data demonstrates that various materials exhibit distinct peak values of susceptibility. The figure also indicates that the susceptibility increases as photon energy increases, likely due to an increase in the number of excited electrons and the given energy value of 2.525 eV for $Fe(phen)_2(SCN)_2$ allows us to calculate the corresponding wavelength using the equation λ = hc/E. Hence, the calculated wavelength is approximately 491.4 nm. Similarly, for $(NH_4)_2[Fe(phen)(SCN)_4]$ with an energy of 3.25 eV, the wavelength is approximately 381.6 nm. In the case of $(NH_4)_4[Fe(SCN)_6]$ with an energy of 1.97 eV, the wavelength is approximately 629 nm. Lastly, for $[Fe(phen)_3]SO_4$) with an energy of 2.345 eV, the wavelength is approximately 529.5 nm as

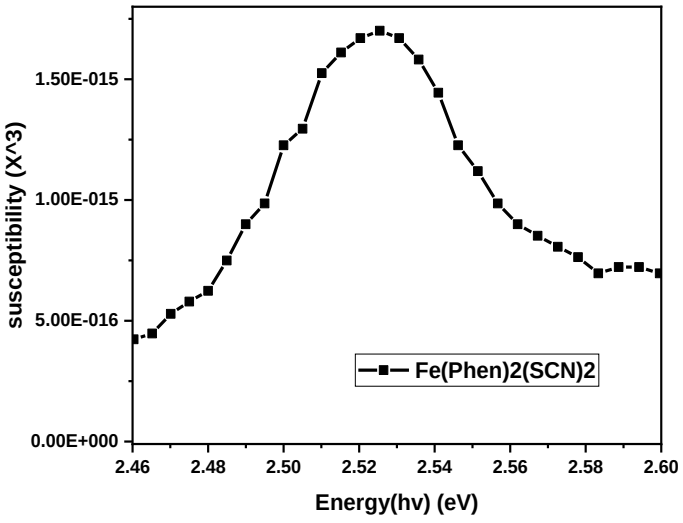

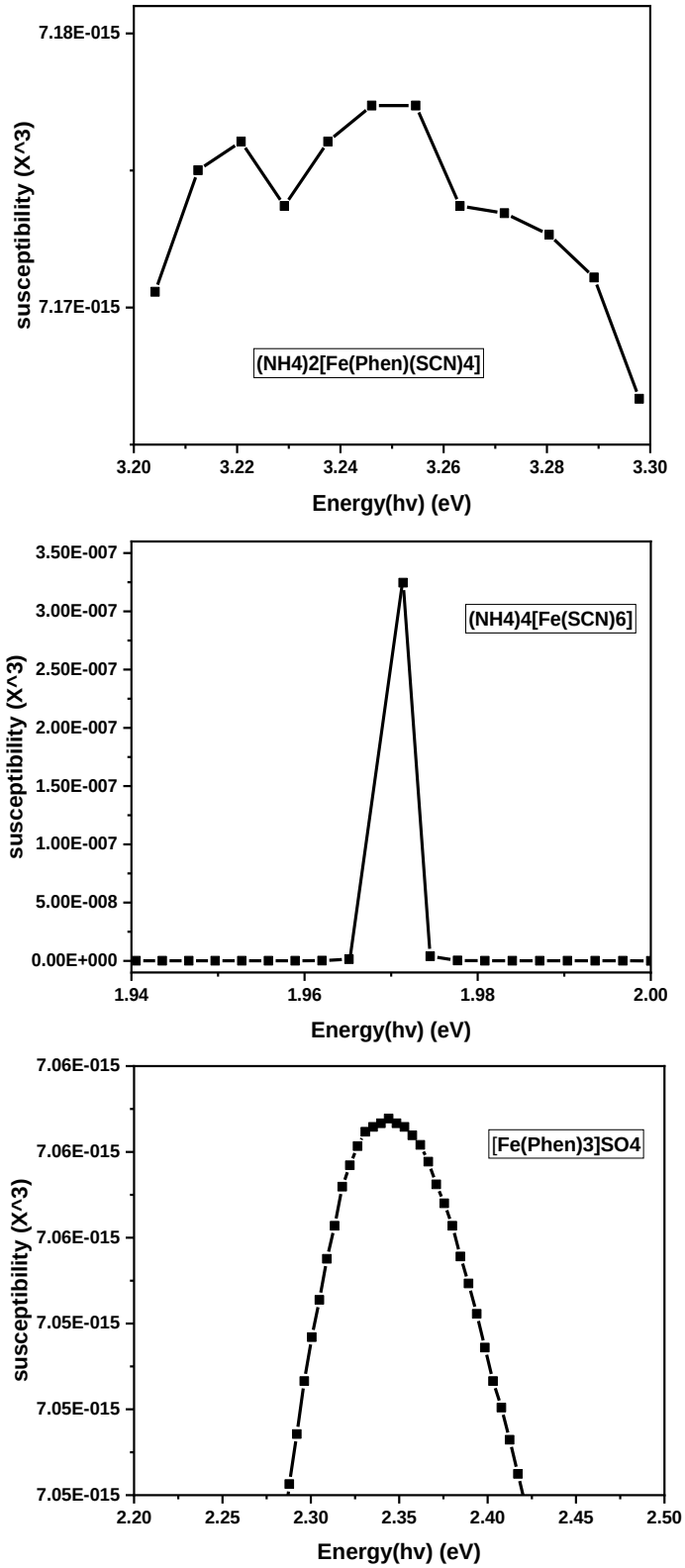

Figure 9: *The relationship of the third order nonlinear optical susceptibility and photon energy*

4. Nonlinear Optical Properties in Spin Crossover (SCO) Compounds

The third-order nonlinear optical susceptibility ($\chi^{(3)}$) describes the response of a material to an intense electromagnetic field, and it is related to the electronic properties of the material. $Iron\ (phen)$ is a complex that exhibits spin transition, which is the switching of the iron ion between two states with different spin configurations .The spin transition in $iron\ (phen)$ alters the electronic structure of the complex and can lead to changes in the energy levels of the electrons. These changes, in turn, can affect the $\chi^{(3)}$ value of the complex [21][22]. In the low-spin (LS) state, the electronic structure of the $iron\ (phen)$ complex is relatively simple, with only a few electronic transitions contributing to the nonlinear response. However, in the high-spin (HS) state, the electronic structure becomes more complex, with many additional electronic transitions contributing to the $\chi^{(3)}$ value [23]. As a result, the spin transition in $iron\ (phen)$ can lead to a significant increase in the $\chi^{(3)}$ value of the complex. This effect has been observed in experiments, where the $\chi^{(3)}$ value of iron (phen) was found to increase by several orders of magnitude when the iron ion underwent a spin transition. Finally, the spin transition in $iron\ (phen)$ can alter the electronic properties of the complex and, in turn, affect its $\chi^{(3)}$ value. This effect is due to changes in the energy levels of the electrons and the number of electronic transitions contributing to the nonlinear response [24].

5. Conclusion

Iron 1,10-phenanthroline molecular nanolayers were synthesized using complexation reactions method. Fe^{2+}(Phen) molecular thin films were then prepared from these nanolayers as samples. The prepared thin films were subjected to characterization using XRD and UV-Vis spectroscopy to investigate their optical properties, thickness of the thin film was measured with a profile meter, and absorbance, transmittance, and reflectivity were measured by $UV-Vis$ spectrophotometer. Four iron ionat thicknesses (100 nm) were measured. The single oscillator model governs the dispersion of the refractive index in the film, the oscillator parameters were determined using this approach, and the direct energy gap (E_g^{WDD}) was computed using the $Wemple-DiDomenico$ approximation, and the third order nonlinear optical susceptibility ($\chi^{(3)}$) was measured using Miller's formula. The optical band is studied using the absorption spectrum, and the direct energy gap was computed using several approaches such as Tauc's relation (E_g^T), Absorption, localized tail states, the concepts of Urbach energy (Eu) and bandgap were thoroughly discussed, and the Urbach energy (Eu) value was obtained by calculating the gradient, as illustrated in Figure 7.The computed values of the energy gap using the various methodologies indicated in Table 3 that the $Fe(phen)_2(SCN)_2$ has a smaller energy gap compared with other molecules. The value of nonlinear optical susceptibility ($\chi^{(3)}$) suggested that the novel polymer might be widely utilized in a variety of photonic electronic applications. As for the optical absorption coefficient, it was found that it increases rapidly with increasing photon energy, which gives a clear indication of the possibility of using it in the fields of commercial optical communications and electronic industry fields such as electrical circuits that it is used in modern devices such as electronic calculators, electron microscopes, electrical switches, and optical imaging. The spin transition in $iron\ (phen)$ can alter the electronic properties of the complex and, in turn, affect its $\chi^{(3)}$ value. This effect is due to changes in the energy levels of the

electrons and the number of electronic transitions contributing to the nonlinear response.

Data availability statement: The whole data of this research is included in this article.

Declaration of competing interest: The authors declare that they have no known competing financial interests or personal relationships that could have appeared to influence the work reported in this paper.

References

1. A. Bencini and V. Lippolis, "1, 10-Phenanthroline: A versatile building block for the construction of ligands for various purposes," *Coord. Chem. Rev.*, vol. 254, no. 17–18, pp. 2096–2180, 2010.
2. J.-F. Létard, P. Guionneau, and L. Goux-Capes, "Towards spin crossover applications," in *Spin Crossover in Transition Metal Compounds III*, 2004.
3. J. E. Monat and J. K. McCusker, "Femtosecond excited-state dynamics of an iron (II) polypyridyl solar cell sensitizer model," *J. Am. Chem. Soc.*, vol. 122, no. 17, pp. 4092–4097, 2000.
4. A. Hauser, "Ligand field theoretical considerations," *Spin Crossover Transit. Met. Compd. I*, pp. 49–58, 2004.
5. P. Gütlich, H. A. Goodwin, and Y. Garcia, *Spin crossover in transition metal compounds I*, vol. 1. Springer Science \& Business Media, 2004.
6. S. Decurtins, P. Gütlich, C. P. Köhler, H. Spiering, and A. Hauser, "Light-induced excited spin state trapping in a transition-metal complex: The hexa-1-propyltetrazole-iron (II) tetrafluoroborate spin-crossover system," *Chem. Phys. Lett.*, vol. 105, no. 1, pp. 1–4, 1984, doi: 10.1016/0009-2614(84)80403-0.
7. A. Hauser, "Intersystem crossing in the [Fe (ptz) 6](BF4) 2 spin crossover system (ptz= 1-propyltetrazole)," *J. Chem. Phys.*, vol. 94, no. 4, pp. 2741–2748, 1991.
8. J. J. McGravey and I. Lawthers, "Photochemically-induced perturbation of the 1 A⇌ 5 T equilibrium in Fe 11 complexes by pulsed laser irradiation in the metal-to-ligand charge-transfer absorption band," *J. Chem. Soc. Chem. Commun.*, no. 16, pp. 906–907, 1982.
9. H. T. Lemke *et al*., "Coherent structural trapping through wave packet dispersion during photoinduced spin state switching," *Nat. Commun.*, vol. 8, no. 1, p. 15342, 2017.
10. C. Bressler *et al*., "Femtosecond XANES study of the light-induced spin crossover dynamics in an iron (II) complex," *Science (80-.).*, vol. 323, no. 5913, pp. 489–492, 2009.
11. A. Al-Hilo *et al*., "2-D and mott transition studies on metal (M) doped PrBa2Cu 3O7," *J. Low Temp. Phys.*, vol. 173, no. 3–4, pp. 89–105, 2013, doi: 10.1007/s10909-013-0893-7.
12. F. A. Kasim, M. A. Mahdi, J. J. Hassan, and S. J. Kasim, "Preparation and optical properties of CdS / Epoxy nanocomposites," vol. 5, pp. 57–66, 2012.
13. W. C. Tan, K. Koughia, J. Singh, and S. O. Kasap, "Fundamental optical properties of materials I," *Opt. Prop. Condens. matter Appl.*, vol. 6, p. 1, 2006.
14. J. I. Pankove, *Optical processes in semiconductors*. Courier Corporation, 1975.
15. H. \cSAFAK, M. Merdan, and Ö. F. Yüksel, "Dispersion analysis of SnS and SnSe," *Turkish J. Phys.*, vol. 26, no. 5, pp. 341–348, 2002.
16. H. M. Jabbar, "Optical Properties of vanadium pentoxide prepared by sol gel method," *J. Kufa-Physics*, vol. 10, no. 01, 2018.
17. S. Il\ican, M. Zor, Y. Ça\uglar, and M. Ça\uglar, "Optical characterization of the CdZn (S1-xSex)(2) thin films deposited by spray pyrolysis method," 2006.
18. H. Fujiwara, *Spectroscopic ellipsometry: principles and applications*. John Wiley \& Sons, 2007.
19. H. M. Jabbar, E. M. Jaboori, and A. Q. Abdullah, "Dispersion parameters, optical constant and photoluminescence of poly vinyl alcohol grafted eosin-Y dye (PVA-g-Ei)," *J. Basrah Res.(Sci.)*, vol. 36, pp. 9–16, 2010.
20. H. B. Tarikhum, F. Almyahi, and B. Ali, "Optical, Structural, and Electrochemical Properties of P3HT:Y6 Photoactive Layer for Organic Photovoltaics," *Karbala Int. J. Mod. Sci.*, vol. 9, no. 4, pp. 618–627, 2023, doi: 10.33640/2405-609X.3328.
21. C. R. Nayar and R. Ravikumar, "Second order nonlinearities of Schiff bases derived from salicylaldehyde and their metal complexes," *J. Coord. Chem.*, vol. 67, no. 1, pp. 1–16, 2014.
22. T. Yang, M. Kurmoo, and M.-H. Zeng, "Recent advances of single-crystal to single-crystal transformation for discrete coordination compounds," *J. Indian Inst. Sci.*, vol. 97, pp. 299–309, 2017.
23. H. A. Badran, A. A. Al-Fregi, R. K. F. Alfahed, and A. S. Al-Asadi, "Study of thermal lens technique and third-order nonlinear susceptibility of PMMA base containing 5′, 5″-dibromo-o-cresolsulfophthalein," *J. Mater. Sci. Mater. Electron.*, vol. 28, pp. 17288–17296, 2017.
24. D. N. Christodoulides, I. C. Khoo, G. J. Salamo, G. I. Stegeman, and E. W. Van Stryland, "Nonlinear refraction and absorption: mechanisms and magnitudes," *Adv. Opt. Photonics*, vol. 2, no. 1, pp. 60–200, 2010.